Armin Darvish[1]
Jung Soo Lee[2]
Bin Peng[2]
Jugal Saharia[2]
Ramalingam Venkat
Kalyana Sundaram[1,3]
Gaurav Goyal[4]
Nuwan Bandara[2]
Chi Won Ahn[5]
Jungsuk Kim[6]
Prashanta Dutta[7]
Irwin Chaiken[3]
Min Jun Kim[2]

[1]School of Biomedical Engineering, Science and Health Systems, Drexel University, Philadelphia, PA, USA
[2]Department of Mechanical Engineering, Southern Methodist University, Dallas, TX, USA
[3]Department of Biochemistry and Molecular Biology, Drexel University College of Medicine, Philadelphia, PA, USA
[4]Quantum Biosystems Inc, Menlo Park, CA, USA
[5]Nano-Materials Laboratory, National NanoFab Center, Daejeon, Republic of Korea
[6]Department of Biomedical Engineering, Gachon University, Incheon, Republic of Korea
[7]School of Mechanical and Materials Engineering, Washington State University, Pullman, WA, USA

Received July 20, 2018
Revised August 13, 2018
Accepted August 14, 2018

Research Article

Mechanical characterization of HIV-1 with a solid-state nanopore sensor

Enveloped viruses fuse with cells to transfer their genetic materials and infect the host cell. Fusion requires deformation of both viral and cellular membranes. Since the rigidity of viral membrane is a key factor in their infectivity, studying the rigidity of viral particles is of great significance in understating viral infection. In this paper, a nanopore is used as a single molecule sensor to characterize the deformation of pseudo-type human immunodeficiency virus type 1 at sub-micron scale. Non-infective immature viruses were found to be more rigid than infective mature viruses. In addition, the effects of cholesterol and membrane proteins on the mechanical properties of mature viruses were investigated by chemically modifying the membranes. Furthermore, the deformability of single virus particles was analyzed through a recapturing technique, where the same virus was analyzed twice. The findings demonstrate the ability of nanopore resistive pulse sensing to characterize the deformation of a single virus as opposed to average ensemble measurements.

Keywords:
Human immunodeficiency virus / Mechanical characterization / Resistive pulse / Solid-state nanopore / Viral maturity
DOI 10.1002/elps.201800311

Additional supporting information may be found online in the Supporting Information section at the end of the article.

1 Introduction

Lipid vesicles are involved in many basic biological processes, such as membrane trafficking, cell endo- and exo-cytosis, and in numerous pathological functions such as virus fusion and entry. The functionality of the vesicles relies on the deformation of the lipid bilayer membrane. For example, fusion of enveloped viruses with the target cells leads to significant membrane distortion and reformation [1]. Studying the membrane deformation mechanism by characterizing the mechanical properties is crucial for understanding the infectivity of viruses.

Correspondence: Dr. Min Jun Kim, Department of Mechanical Engineering, Southern Methodist University, Dallas, TX 75275, USA
Fax: +1-214-768-1473
E-mail: mjkim@lyle.smu.edu

Abbreviations: AFM, atomic force microscopy; **HIV**, human immunodeficiency virus; **MBCD**, methyl-β-cylcodextrin; **TEM**, transmission electron microscopy

In the past decades, a variety of techniques, including micropipette aspiration [2], fluctuation analysis [3], atomic force microscopy (AFM) [4, 5], optical tweezers [6], and electrodeformation [7], have been used to measure the bending rigidity of membranes. While the bending rigidity of the planar bilayers [8, 9], giant vesicles [7], and cells [10, 11] have been widely studied [12, 13], little is known about the membrane mechanics at the nanoscale. Most of the above-mentioned techniques rely on the direct visualization of membrane deformation with optical microscopy and, thus, cannot be applied to nanoscale vesicles where direct visualization is not possible due to the light diffraction limit. Other techniques, such as super-resolution microscopy and electron microscopy, can overcome the light diffraction limit and resolve nanoscale features but they cannot visualize the dynamics of the membrane deformation under physiological conditions. Currently, AFM is the popular choice for direct measurement of deformation at the nanoscale [14], but analyzing small nanoscale vesicles

Color Online: See the article online to view Figs. 1–4 in color.

in solution with AFM is a demanding task. The object must be chemically immobilized on a flat and rigid surface; this can alter the mechanical properties of the membrane by causing flattening and deformation. In addition, probing soft vesicles with the AFM tip can drag the vesicles, or even rupture their membranes. While recent advances have addressed some of these drawbacks [15–17], a more important limitation of AFM is its intrinsic low throughput. The operator must scan the field of view at high resolutions to find single nanoscale particles before proceeding with measurements, which is a cumbersome and time-consuming process. In fact, many AFM studies on nanoscale vesicles report data on a low number (<100) of samples [18, 19], which is statistically insignificant considering the intrinsic heterogeneity of biological or synthetic vesicles. AFM measurements of so few particles can be challenging to establish meaningful correlations between the mechanical properties and the biological functions.

In the proof-of-the-principle experiments, we demonstrated that nanopore resistive pulse sensing technique can be used to compare the deformation behavior of synthetic liposomes [20, 21]. Here, we use human immunodeficiency virus (HIV-1) as model systems to demonstrate the applicability for biological samples. A thin membrane that contains a single nanopore is placed between two chambers (*cis* and *trans* chambers), which are filled with an electrolyte solution, and a bias voltage is applied across the membrane. Virus-containing solutions are then added to one side of the membrane. The electrophoretic forces acting on negatively charged viruses cause translocations through the pore. When a single vesicle translocates through the pore, it changes the resistance of the pore and causes a transient resistive pulse in the ionic current. Since the electric field is locally amplified within the nanopore, it creates a region of strong electric field that can cause electrodeformation of viral particles. The characteristics of resistive pulse, the amplitude and duration, can therefore be used to describe the extent of viral particle deformation. While several groups have used nanopores for characterization of biological nanoparticles, such as exosomes [22, 23] and viruses [24–26], the possible deformation of these particles inside nanopores and the resultant effects on particle characterization have been widely neglected.

HIV-1 is particularly selected as the model system because its mechanical properties have already been characterized by AFM, and a potential link between the mechanical properties and the pathobiological functions have been identified [18, 27]. It has been shown that softer mature viruses are more infective than stiff immature ones, which can be explained by the structural differences between the two variants. In the immature state, the Gag protein forms a thick shell underneath the viral membrane, rendering the stiffness of the virus. During maturation, this thick shell is proteolytically cleaved into a conical thin shell called viral capsid, hence, the virus becomes softer and gains its infectivity. In addition, it was reported that the number of envelop proteins in mature viruses has no effect on the stiffness of HIV-1 [18, 27]. Therefore, HIV-1 provides a good model to assess our nanopore-based technique in analyzing the mechanical properties of biological particles at the nanoscale. In this report, we analyzed the resistive pulse events of HIV-1 virus particles as they passed through nanopores and used it to study virus deformation and distinguish viruses of different structures (i.e. mature vs. immature). In addition, the effect of cholesterol removal from viral membrane was studied since cholesterol has been shown to affect the rigidity of membranes [3, 5, 7, 9]. Cholesterol removal from viral membrane was achieved by methyl-β-cyclodextrin (MBCD) treatment [28], which has been shown to diminish viral infectivity [29, 30].

2 Materials and methods

2.1 Reagents

MBCD powder was purchased from Sigma Aldrich (St. Louis, MO, USA). 293 T cells were obtained from American Type Culture Collection (Manassas, VA, USA) and were grown in DMEM supplemented with 10% fetal bovine serum, 2.5% HEPES, 1% Penicillin-Streptomycin and 2% L-Glutamine. DNA plasmids, HIV-$1_{BaL.01}$ Env and NL4-3 R^- E^- Luc^+ as well as HIV antibodies were obtained from NIH AIDS reagents program, division of AIDS, NIAID (kind gifts from Dr. John Mascola and Dr. Nathaniel Landau, respectively). All other reagents were purchased from Fisher Scientific (Hampton, NH, USA).

2.2 Virus production and purification

HIV-1 pseudoviruses were produced following the co-transfection method reported elsewhere [29, 31] Detailed procedures can be found in the Supporting Information (Section 2) and the schematic in Supporting Information Fig. 2. All pseudovirus samples were tested for p24 content, gp120 expression and infectivity as reported before [29, 31]. All samples were aliquoted and kept in freezer at -80°C until further use.

2.3 Transmission electron microscopy (TEM)

Virus samples were fixed in aqueous solution containing 1% of Paraformaldehyde and 0.1% of Glutaraldehyde at 4°C for 15 min and washed once using a desktop centrifuge at 2000 g for 3 min in Amicon concentrators (100 kDa MWCO). Then, they were mixed with 1% of osmium tetroxide and incubated with gentle shaking at 4°C for 1 h before being washed again for seven times with DI water. The samples were then concentrated to 100 μL volume and loaded on holey carbon grids (purchased from EM Microscopy) and dried overnight. Just before the TEM imaging, samples were stained with 0.1% Uranyl Acetate and rinsed. Imaging was performed with a JEOL 2100 transmission electron microscope at 120 keV accelerating voltage.

2.4 Nanopore resistive pulse sensing

The nanopore chip (fabrication outlined in Section 1 of Supporting Information) was thoroughly cleaned using piranha solution at 80°C for ~10 min. The chip was then sealed by sandwiching it between two PDMS gaskets using an in-house built polycarbonate flow cell. The *cis* and *trans* chambers of the flow cell were filled with an electrolyte aqueous solution (10mM PBS, 140mM KCl, pH 7.4). A Molecular Devices (San Jose, CA, USA) Axopatch 200B amplifier was used with Ag/AgCl electrodes to record signals. The current was measured at a sampling frequency of 200 kHz and filtered by an inbuilt 10 kHz low-pass Bessel filter. The signal was digitized with a Molecular Devices Digidata 1440A digitizer. The pore conductance was tested with the open current before loading sample in the *cis* chamber to ensure that the conductance of the pore was the same as before and no trace of contaminants from previous experiments was left in the pore or flow cells. The size of the pore was estimated using a solution-based conductance model [32, 33],

$$G = \sigma\left[\frac{4L}{\pi D^2} + \frac{1}{D}\right]^{-1} \quad (1)$$

where D is nanopore diameter, L is length and σ is the conductivity of the electrolyte solution. The experiments were done with two unique nanopores comparable in size and conductance. As shown in the Supporting Information Fig. 1b), both pores were about 250 nm in diameter.

For virus translocation experiments, vials of mature HIV-1 Bal.01 viruses were thawed and mixed with PBS (10 mM, pH = 7.4) solution in 1:1 ratio. To remove cholesterol from the viral membrane, 5 mM MBCD in PBS was used instead of PBS. The samples were then incubated for 30 min at 37°C before they were washed twice with PBS at 2000 g for 3 min in Amicon concentrators (100 kDa MWCO). Immature viruses were prepared similar to mature samples. Vials of Δpro viruses were thawed and treated with PBS in a 1:1 ratio and incubated for 30 min at 37°C before washing with PBS twice. A 50 μL aliquot of as-prepared samples were immediately added to the *cis* chamber of the flow cell and the current was recorded until over 1000 events were collected for each sample at each applied voltage.

2.5 Signal processing

All signal processing and data plotting was done using custom-written scripts of MATLAB and graphical interfaces (Supporting Information Fig. 3). A moving average method was used to correct any baseline drifts [34]. Events were classified as current perturbations six times the standard deviation of the baseline current. Each event was then characterized in terms of amplitude, FWHM duration and relative peak amplitude ($\Delta I/I_0$, with ΔI and I_0 the current magnitude of the event and the baseline current). The peak of the Gaussian fit made to the histogram of amplitude of events was treated as the average peak amplitude for each sample (Supporting Information Fig. 4).

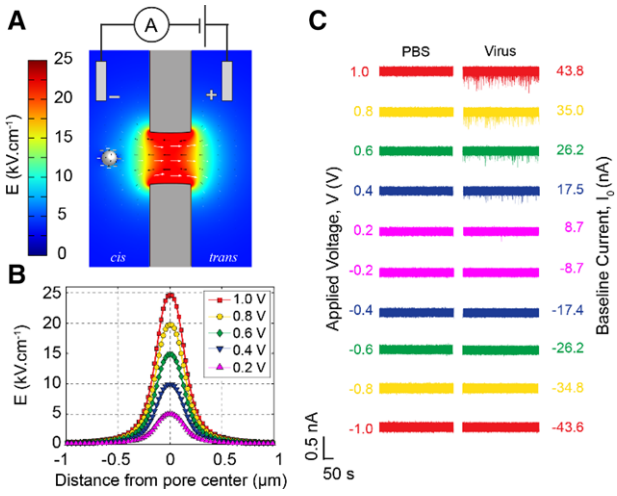

Figure 1. (A) Schematic of virus translocation through nanopores. The color gradient shows the magnitude of electric field obtained from finite element simulation using COMSOL. The arrows show ionic flux through the nanopore. (B) Voltage-dependent electric field profiles near a nanopore without any particle calculated by the finite element simulation in COMSOL. (C) Representative current trace of virus sample and the negative control. Mature HIV-1 pseudostype virus was used.

3 Results and discussion

3.1 Virus detection by resistive pulse sensing

HIV-1 particles dispersed in PBS (10 mM, pH = 7.4) were added to the *cis* chamber in our experimental setup reported elsewhere [20, 21, 33, 35, 36]. Upon grounding the *cis* chamber and applying a positive voltage bias across the nanopore, we observed perturbations in the current trace more formally defined as resistive pulses or events (Fig. 1. See Section 2.5 for event classification). Figure 1A illustrates the working principle of resistive pulse sensing; negatively charged viruses were driven through the pore by the electric field in and around the pore. Each resistive pulse is indicative of a single HIV virus translocating through the pore. Further proof for translocation is provided through the recapturing process where a particle translocating through the nanopore to the particle-free reservoir is translocated back through the nanopore by instantaneous voltage reversal. The color gradient in Fig. 1A shows the magnitude of the electric field calculated by a finite element simulation in COMSOL (see Section 4 of Supporting Information). A negatively charged virus is electrophoretically driven though the nanopore. The magnitude of the field was linearly dependent on the applied bias voltage (Fig. 1B). Therefore, as the applied voltage was increased, the electric force that pulls the viral particles through the nanopore became stronger and higher capture rates were observed (Fig. 1C). However, at negative voltage

bias, no resistive pulses were detected due to charge repulsion (Fig. 1C). The negative control (PBS buffer with no virus) did not show any resistive pulse signals at any applied voltages. Ability to detect virus translocation significantly diminished when the applied voltage was decreased. This behavior is expected because at lower voltages lower electrophoretic forces are imparted on the molecule. Based on these findings, the following experiments were carried out at voltages higher than 0.4 V and capped at 1 V due to instrumental limitation of the Axopatch amplifier used in our experimental setup.

3.2 Size and structure of virus variants

Once we established the ability to sense HIV-1 with nanopore sensors, we focused on mechanical characterizations of the viruses. As demonstrated in our previous works [20, 21], soft nanoparticles can undergo significant electrodeformation as they pass through nanopores. The extent of electrodeformation can be characterized by comparing $\Delta I/I_0$ of the resistive pulses. While the exact underlying mechanism for the electrodeformation in nanopores is yet to be understood, the technique can offer a relatively cheap, user-friendly and high-throughput alternative to AFM, for studying the deformation behaviors of lipid vesicles at the nanoscale.

A panel of HIV-1 including immature and mature viruses with various amounts of envelope protein (Env) expression were prepared according to protocols reported previously (see methods section and Section 2 of Supporting Information for more details). Furthermore, we analyzed mature HIV-1 treated with 5 mM MBCD. MBCD treatment is widely used for cholesterol depletion [28]. Since our previous works have shown that cholesterol depletion from HIV-1 membrane reduces the energy barrier to fusion between virus and cell membranes [29], we expected the MBCD-treatment to be further soften the mature virus. Altogether a panel of viruses including: 1-immature virus, 2-mature virus with no Env, 3-mature virus with 1x Env, 4-mature virus with 4x Env, and 5-MBCD treated mature virus provide a range of samples with varied rigidities for our study.

Figure 2A shows TEM images of all the virus samples used in this work. Average diameters of viruses were measured from these TEM images and a Gaussian distribution was fitted to the histograms with the peak representing the average size of viruses in each sample (Fig. 2B). All samples showed an average size of ~100 nm in diameter, which is in agreement with values reported in the literature [37–39]. The insets in Fig. 2B show a schematic representation of the virus structure. Furthermore, the amount of Env protein on all mature virus types were confirmed by immunogold tagging of viruses and TEM imaging (see Supporting Information Fig. 2d for more details).

3.3 Electrodeformation of viruses in nanopores

All variants of HIV-1 samples yielded resistive pulses through nanopore sensing. A representative current trace and a single event are shown for each sample (Fig. 2C and D). The immature particles yielded a larger peak amplitude (ΔI) than the other three variants of mature particles. This result was expected since mature variants are softer than immature viruses and as seen in Supporting Information Fig. 5, they perturb the ionic flow less compared to a rigid particle. The MBCD-treated mature particles resulted in the smallest spikes of all the samples. This is not surprising as MBCD causes cholesterol depletion which can lead to particle softening. Since the original sizes of the variants are similar to each other based on TEM images (Fig. 2A, Supporting Information Fig. 2d), the differences in peak amplitude between the variants are not from the size differences but rather from differences in membrane rigidity, as discussed in the following sections.

The extent of electrodeformation of a particle inside a nanopore can be characterized by $\Delta I/I_0$ of the resistive pulse. A voltage-dependent trend is expected if the particles are deformed by the electrohydrodynamics inside a nanopore [20]. Consequently, resistive pulse characterization was done from 0.4 to 1 V applied voltage bias using two unique nanopores of comparable size (Supporting Information Fig. 1). Each experiment was triplicated. Figure 3A compares the $\Delta I/I_0$ for different virus samples. As the voltage is increased, the relative peak amplitude ($\Delta I/I_0$) decrease, suggesting that the viruses were deforming as they were translocating through nanopores similar to what was previously observed for liposomes [20, 21]. As expected, the dependence of relative peak amplitude on applied voltage varies for different HIV-1 variants.

3.4 Computational modeling of virus deformation

A recent molecular dynamic modelling of micelle translocation through nanopores showed a stretching effect [40] similar to what we have proposed for liposomes and viruses, which confirms soft particle deformation in nanopores. The larger dimensions and longer time-scale of virus translocation experiments in this work, however, is beyond the limits of molecular dynamics modelling and therefore molecular dynamics was not suitable to simulate virus translocations. Instead, a quasi-steady state simulation was used to model the resistive pulse signals of virus translocations following methods described in the literatures [20, 41] (See Section 4 of Supplementary Information for more details). Elongated ellipsoidal geometries were used to model deformed particles, assuming the overall volume of the particles is conserved (Supporting Information Fig. 5). Following the methods reported previously [20], the effective aspect ratio (l/r, Supporting Information Fig. 5c) of the deformed particles were calculated. In short, the $\Delta I/I_0$ for particles with aspect ratios (l/r) between 1 and 4 were modelled and the relative peak amplitude to effective aspect ratio was constructed by interpolating the standard curve (Supporting Information Fig. 5c). The experimentally measured values for relative peak amplitudes were then used to estimate the effective aspect ratio of

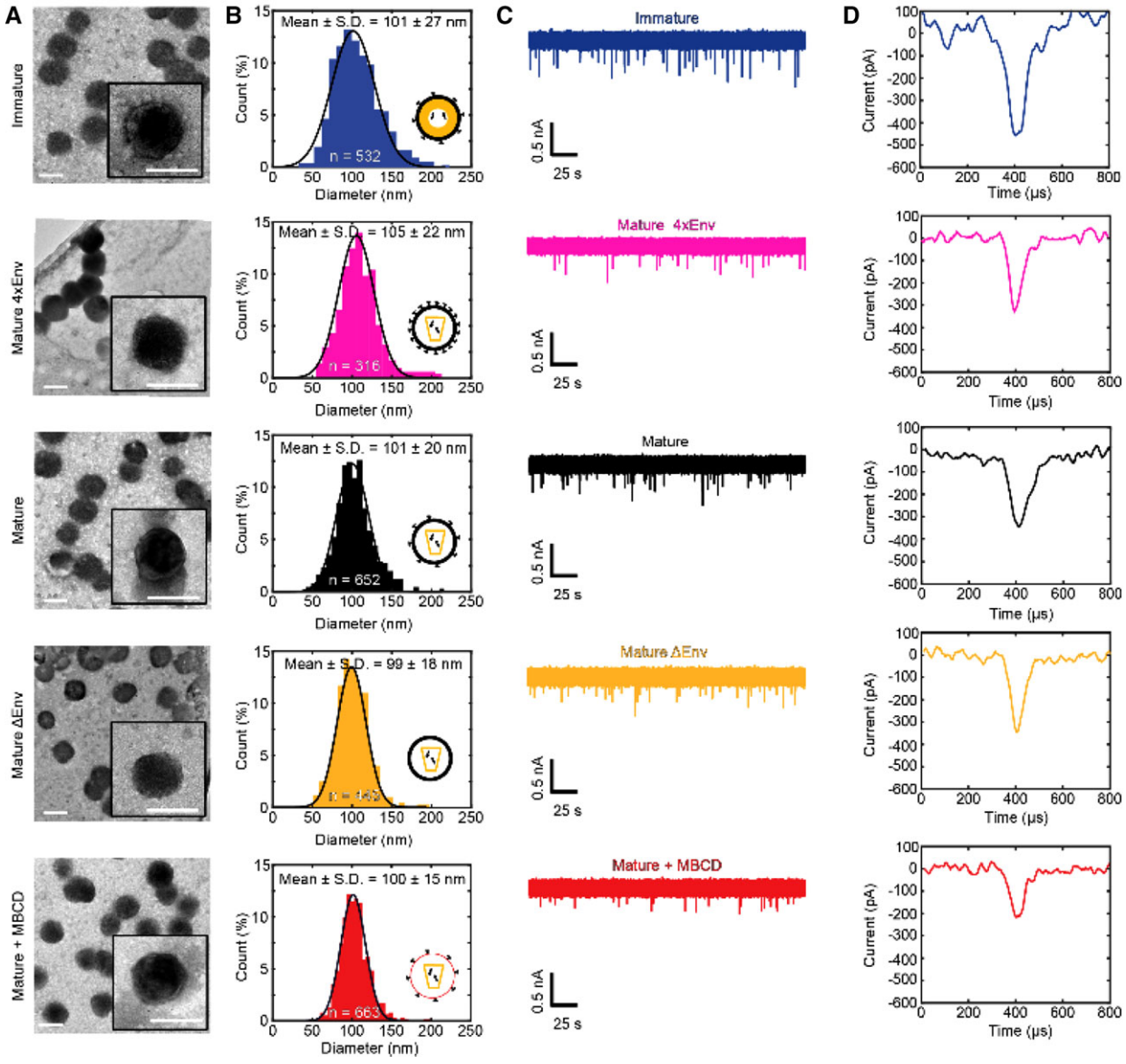

Figure 2. (A) TEM micrographs of all different virus samples. All scale bars are 100 nm. (B) Histograms of the virus diameter measured from the TEM micrographs. The black curves are Gaussian fittings. The total counts are written in white color. The insets show schematics of each viral structure. (C) Representative current traces for various virus samples. (D) Representatives of a single extracted resistive pulse event for each sample.

the deformed viruses from this standard curve. The results are shown in Fig. 3B. As can be seen, immature viruses underwent the least amount of deformation followed by mature viruses. The deformations of all mature variants of viruses were similar, which means the rigidity of the mature viruses were independent of the amount of Env expression. These results agree with findings from AFM studies of immature and mature viruses [18,27]. Interestingly, the cholesterol-depleted viruses showed the highest amount of deformation, suggesting that cholesterol depletion decreased the rigidity of the viruses. This finding can explain the lower energy barrier to fusion/lysis observed previously [29].

3.5 Single virus deformation analysis by recapturing

While the method introduced so far can compare the mechanical properties of viruses and vesicles, it is still an average ensemble method that compares the average values of bulk measurements. The characteristics of the resistive pulses and the estimated aspect ratios above, represent the average values for all viruses and does not describe the subpopulation variations. Since the heterogeneity in particle size was observed (20% variation in virus diameter) under TEM (Fig. 2A), the calculated aspect ratios can show errors due to averaging. Hence, single-particle measurements, where

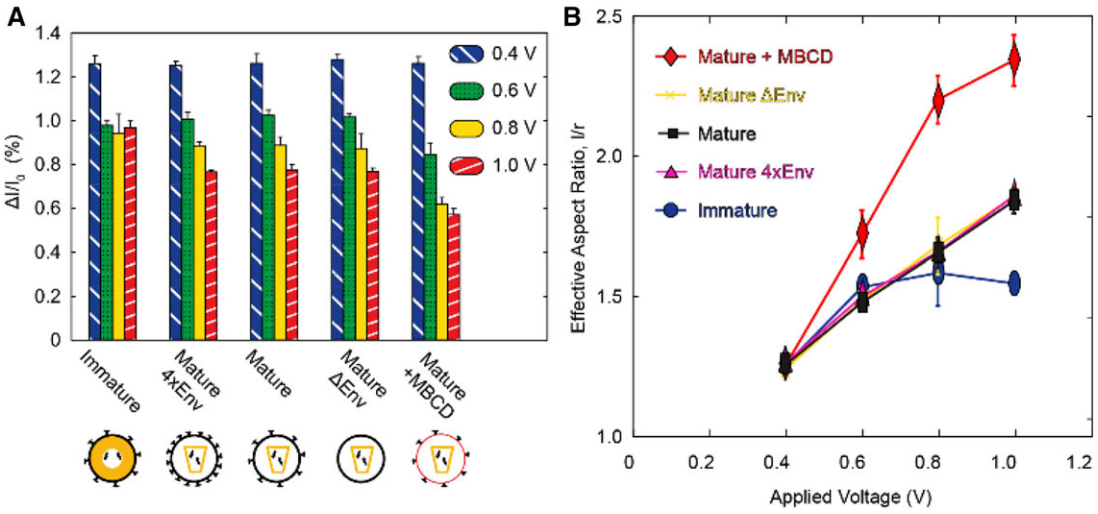

Figure 3. (A) Bar graphs of relative peak amplitudes, the ratio of current drop amplitude (ΔI) divided by open-channel baseline current (I_0), for each sample at each applied voltage (B) Estimated effective aspect ratios of the viruses, calculated from finite element simulations.

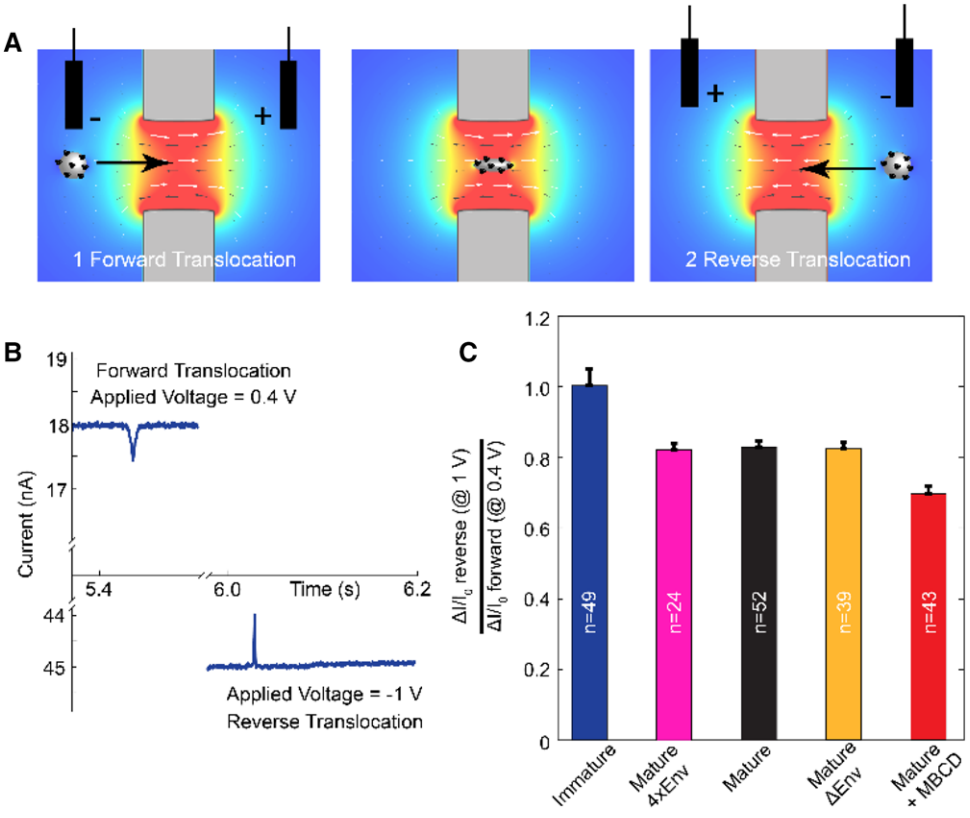

Figure 4. (A) Illustration of a recapture experiment (B) An example of current trace for recapturing showing both forward and reverse translocation events (C) The ratio of relative peak amplitudes in forward direction (1 V) to reverse direction (0.4 V) for the recapture events. The number on the bar represents the sample size of viruses for each category.

each particle is compared to itself under two different voltages, are preferred in analyzing virus deformation. To achieve such single-particle measurements, back and forth measurements of a single particle were conducted by recapturing it, which diminishes the negative effect from the intrinsic size variance. The translocating virus was recaptured by changing the direction of the electric field, thereby instantaneously pulling the virus electrophoretically back into the nanopore for a second measurement. This was achieved by manually reversing the applied voltage immediately after a virus translocation was detected (Fig. 4A). This is in essence a nanoscale version of the method used by Zheng *et al.* [42] for measuring

deformability of red blood cells in a microfluidic device. One single particle is deformed inside a nanopore at two different magnitudes of applied forces (electric field strength). The relative value of the two deformations (ratio of the resistive pulse amplitudes) describes the deformability (i.e. rigidity) of the particle.

The deformability of the virus was described by the ratio of the forward relative peak amplitude (*cis* to *trans*, $\Delta I/I_0$ at 0.4 V) to the backward relative peak amplitude (*trans* to *cis*, $\Delta I/I_0$ at -1 V). Figure 4B shows a representative example of a recapture event. Once a resistive pulse at an applied voltage of 0.4 V was observed, the applied voltage was changed to –1.0 V. This abrupt potential switch caused a capacitive charging effect which lasts for a few milliseconds due to charge accumulation on the dielectric silicon nitride membrane (presented as a break on the x-axis of Fig. 4B). As shown in the Fig. 4B, a second resistive pulse was observed in the reverse direction, which potentially marks the recapture event of the same virus. Due to the higher applied voltage in the reverse direction, we were able to observe the shape deformation and faster translocation. The difference in both amplitude and duration of the pulses between forward and reverse direction in Fig. 4B is noteworthy.

When virus samples were loaded into the *cis* side of the flow cell and a negative voltage was applied, no translocation was observed (Fig. 1A), which demonstrated that the resistive pulse signal observed in the reverse direction represents a true recaptured virus. In addition, low concentrations of virus samples in recapture experiments lowered the capture rate in the forward direction, ensuring that the recaptured signals were originated from the same virus sample. The applied voltage in the forward direction (0.4 V) was set lower than the reverse direction (1 V); this made the manual recapture experiment easier to perform due to the slower translocation speed of the virus in the forward direction. Recapture experiments for each sample were performed and the ratio of relative peak amplitudes in reverse vs. forward direction were compared. Figure 4C illustrates the average value of this ratio for all HIV samples. The data suggest that immature viruses retained their shape with almost no deformation. Mature viruses showed some deformation, but no significant difference was observed among the mature viruses with different amounts of Env expression. Cholesterol-depleted viruses showed the most amount of deformation in reverse translocation. This trend agrees with the results observed in the average ensemble studies.

Our findings demonstrate the capability of single-particle studies with nanopore resistive pulse sensing. Since the manual control of the voltage switch has its limitation and can lead to errors, an automated recapture platform using a feedback control system is preferable for future recapture experiments [43–46]. The automated setup can recapture single virus for multiple times, which will allow us to examine large amount of recapturing data from a single analyte conferring the deformability value with higher fidelity.

4 Concluding remarks

The experimental results demonstrated that our solid-state nanopore platform can distinguish between virus particles of different rigidity. We have shown that immature viruses have higher rigidity compared to mature viruses, which is in agreement with findings from AFM [18, 27]. We also showed that cholesterol depletion from viral membranes can further soften mature viruses. This is an important finding since cholesterol depletion has previously been shown to alter virus infectivity and stability [29]. In addition, single-virus measurements were done by reversing the voltage and recapturing the same particle in the nanopore. Such measurements further confirmed the trends we observed in average ensemble measurements. Since the resistive pulse of the same particle was measured at two different voltages in recapturing experiments, the shift in relative peak amplitudes truly represents single particle deformability.

In conclusion, we have demonstrated the ability of nanopores to characterize mechanical properties of viruses at a single-particle level. While the recapture process for single-particle measurements requires further instrumentation and protocol development to overcome some of the current limitations, our work here demonstrated the feasibility of the nanopore sensor for a single virus analyzer, which characterizes mechanical properties of the viral membrane. Upon further improvement and optimization, a platform like our system can open a new technological avenue to investigate the biophysical basis of virus entry, membrane trafficking, and membrane fusion at nanoscale.

This work was financially supported by National Science Foundation (CMMI #1707818 and #1712069), National Institutes of Health (R03EB022759, P01GM56550, and R01GM111029), and National Research Foundation of Korea (NRF-2015K1A4A3047100, NRF-2015M3A7B6027973, and NRF-2015M3A6B3068660). Also, special thanks should be given to Dr. Chris Aiken in Vanderbilt University, Dr. John Mascola and Dr. Nathaniel Landau in NIH AIDS reagents program for providing invaluable biological samples.

The authors have declared no conflict of interest.

5 References

[1] Chernomordik, L. V., Kozlov, M. M., *Nat. Struct. Mol. Biol.* 2008, *15*, 675–683.

[2] Evans, E., Needham, D., *J Phys Chem.-Us* 1987, *91*, 4219–4228.

[3] Henriksen, J., Rowat, A. C., Ipsen, J. H., *Eur. Biophys. J. Biophy* 2004, *33*, 732–741.

[4] Garcia-Manyes, S., Sanz, F., *Biochim. Biophys. Acta* 2010, *1798*, 741–749.

[5] Liang, X. M., Mao, G. Z., Ng, K. Y. S., *J. Colloid Interf. Sci.* 2004, *278*, 53–62.

[6] Ou-Yang, H. D., Wei, M. T., *Annu. Rev. Phys. Chem.* 2010, *61*, 421–440.

[7] Gracia, R. S., Bezlyepkina, N., Knorr, R. L., Lipowsky, R., Dimova, R., *Soft Matter* 2010, *6*, 1472–1482.

[8] Attwood, S. J., Choi, Y., Leonenko, Z., *Int. J. Mol. Sci.* 2013, *14*, 3514–3539.

[9] Redondo-Morata, L., Giannotti, M. I., Sanz, F., *Langmuir* 2012, *28*, 12851–12860.

[10] Evans, E. A., *Biophys. J.* 1983, *43*, 27–30.

[11] Cross, S. E., Jin, Y. S., Rao, J., Gimzewski, J. K., *Nat. Nanotechnol.* 2007, *2*, 780–783.

[12] Booth, P. J., Riley, M. L., Flitsch, S. L., Templer, R. H., Farooq, A., Curran, A. R., Chadborn, N., Wright, P., *Biochemistry-Us* 1997, *36*, 197–203.

[13] Saleem, M., Morlot, S., Hohendahl, A., Manzi, J., Lenz, M., Roux, A., *Nat. Commun.* 2015, *6*.

[14] Delorme, N., Fery, A., *Phys. Rev. E* 2006, *74*.

[15] Zhao, B. Y., Song, Y., Wang, S., Dai, B., Zhang, L. J., Dong, Y. M., Lu, J. H., Hu, J., *Soft Matter* 2013, *9*, 8837–8843.

[16] Chopinet, L., Formosa, C., Rols, M. P., Duval, R. E., Dague, E., *Micron* 2013, *48*, 26–33.

[17] Monserrate, A., Casado, S., Flors, C., *ChemPhysChem* 2014, *15*, 647–650.

[18] Kol, N., Shi, Y., Tsvitov, M., Barlam, D., Shneck, R. Z., Kay, M. S., Rousso, I., *Biophys. J.* 2007, *92*, 1777–1783.

[19] Li, S., Eghiaian, F., Sieben, C., Herrmann, A., Schaap, I. A., *Biophys. J.* 2011, *100*, 637–645.

[20] Darvish, A., Goyal, G., Aneja, R., Sundaram, R. V., Lee, K., Ahn, C. W., Kim, K. B., Vlahovska, P. M., Kim, M. J., *Nanoscale* 2016, *8*, 14420–14431.

[21] Goyal, G., Darvish, A., Kim, M. J., *Analyst* 2015, *140*, 4865–4873.

[22] Anderson, W., Lane, R., Korbie, D., Trau, M., *Langmuir* 2015, *31*, 6577–6587.

[23] Maas, S. L. N., de Vrij, J., van der Vlist, E. J., Geragousian, B., van Bloois, L., Mastrobattista, E., Schiffelers, R. M., Wauben, M. H. M., Broekman, M. L. D., Nolte-'t Hoen, E. N. M., *J. Control. Release* 2015, *200*, 87–96.

[24] Arjmandi, N., Van Roy, W., Lagae, L., Borghs, G., *Anal. Chem.* 2012, *84*, 8490–8496.

[25] Arjmandi, N., Van Roy, W., Lagae, L., *Anal. Chem.* 2014, *86*, 4637–4641.

[26] Yang, L., Yamamoto, T., *Front Microbiol.* 2016, *7*, 1500.

[27] Pang, H. B., Hevroni, L., Kol, N., Eckert, D. M., Tsvitov, M., Kay, M. S., Rousso, I., *Retrovirology* 2013, *10*, 4.

[28] Mahammad, S., Parmryd, I., *Methods Mol. Biol.* 2015, *1232*, 91–102.

[29] Kalyana Sundaram, R. V., Li, H., Bailey, L., Rashad, A. A., Aneja, R., Weiss, K., Huynh, J., Bastian, A. R., Papazoglou, E., Abrams, C., Wrenn, S., Chaiken, I., *Biochemistry-Us* 2016, *55*, 447–458.

[30] Campbell, S. M., Crowe, S. M., Mak, J., *AIDS* 2002, *16*, 2253–2261.

[31] Bastian, A. R., Kantharaju, McFadden, K., Duffy, C., Rajagopal, S., Contarino, M. R., Papazoglou, E., Chaiken, I., *ChemMedChem* 2011, *6*, 1335–1339, 1318.

[32] Goyal, G., Freedman, K. J., Kim, M. J., *Anal. Chem.* 2013, *85*, 8180–8187.

[33] Goyal, G., Mulero, R., Ali, J., Darvish, A., Kim, M. J., *Electrophoresis* 2015, *36*, 1164–1171.

[34] Plesa, C., Dekker, C., *Nanotechnology* 2015, *26*, 084003.

[35] Freedman, K. J., Bastian, A. R., Chaiken, I., Kim, M. J., *Small* 2013, *9*, 750–759.

[36] Freedman, K. J., Haq, S. R., Edel, J. B., Jemth, P., Kim, M. J., *Sci. Rep.* 2013, *3*, 1638.

[37] Wilk, T., Gross, I., Gowen, B. E., Rutten, T., de Haas, F., Welker, R., Krausslich, H. G., Boulanger, P., Fuller, S. D., *J. Virol.* 2001, *75*, 759–771.

[38] Briggs, J. A., Wilk, T., Welker, R., Krausslich, H. G., Fuller, S. D., *EMBO J.* 2003, *22*, 1707–1715.

[39] Frank, G. A., Narayan, K., Bess, J. W., Jr., Del Prete, G. Q., Wu, X., Moran, A., Hartnell, L. M., Earl, L. A., Lifson, J. D., Subramaniam, S., *Nat. Commun.* 2015, *6*, 5854.

[40] Restrepo-Pérez, L., John, S., Aksimentiev, A., Joo, C., Dekker, C., *Nanoscale* 2017, *9*, 11685–11693.

[41] Jubery, T. Z., Prabhu, A. S., Kim, M. J., Dutta, P., *Electrophoresis* 2012, *33*, 325–333.

[42] Zheng, Y., Nguyen, J., Wang, C., Sun, Y., *Lab Chip* 2013, *13*, 3275–3283.

[43] Lee, J. S., Peng, B., Sabuncu, A. C., Nam, S., Ahn, C., Kim, M. J., Kim, M., *Electrophoresis* 2018, *39*, 833–843.

[44] Gershow, M., Golovchenko, J. A., *Nat. Nanotechnol.* 2007, *2*, 775–779.

[45] Stein, D., *Nat. Nanotechnol.* 2007, *2*, 741–742.

[46] Plesa, C., Cornelissen, L., Tuijtel, M. W., Dekker, C., *Nanotechnology* 2013, *24*, 475101.

